Energy and Buildings 135 (2017) 398–409

Contents lists available at ScienceDirect

Energy and Buildings

journal homepage: www.elsevier.com/locate/enbuild

Inferring the thermal resistance and effective thermal mass distribution of a wall from in situ measurements to characterise heat transfer at both the interior and exterior surfaces

Virginia Gori [a,*], Valentina Marincioni [b], Phillip Biddulph [a], Clifford A. Elwell [a]

[a] UCL Energy Institute, 14 Upper Woburn Place, London WC1H 0NN, UK
[b] UCL Institute for Environmental Design and Engineering, 14 Upper Woburn Place, London WC1H 0NN, UK

ARTICLE INFO

Article history:
Received 22 August 2016
Received in revised form 20 October 2016
Accepted 22 October 2016
Available online 27 October 2016

Keywords:
External wall
U-value
R-value
Thermal mass
Bayesian statistics
Heat transfer
In situ measurements

ABSTRACT

The estimation of the thermophysical characteristics of building elements based on in situ monitoring enables their performance to be assessed for quality assurance and successful decision making in policy making, building design, construction and refurbishment. Two physically-informed lumped thermal mass models, together with Bayesian statistical analysis of temperature and heat flow measurements, are presented to derive estimates of the thermophysical properties of a wall. The development of a two thermal mass, three thermal resistance model (2TM) enabled the thermal structure of the wall to be investigated and related to the known physical structure of two heavy-weight walls of different construction: a solid brick wall and an aerated clay, plaster, woodfibre insulation and gypsum fibreboard wall. The 2TM model produced good match to the measured heat flux at both interior and exterior surfaces for both walls, unlike a one thermal mass model (1TM); Bayesian model comparison strongly supported the 2TM over the 1TM model to accurately describe the observed data. Characterisation of the thermal structure and performance of building elements prior to decision making in interventions will support the development of tailored solutions to maximise thermal comfort and minimise energy use through insulation, heating and cooling strategies.

1. Introduction

The thermophysical properties of the building envelope have been identified as key parameters in the determination and explanation of the energy performance of buildings and are widely used in models to predict the energy demand of the built stock [1–3]. However, a performance gap has been identified between the expected energy use of buildings and their measured energy use [4–6]. The origins of the performance gap are multi-layered and complex, involving issues such as occupant behaviour, technological performance, construction defects, and changes to the materials and design [5,7].

Deviation between the expected thermophysical performance of building elements from tabulated data and their measured performance has been identified as a significant issue in a number of studies [8–11]. Unlike the use of standard published values, the measurement and analysis of in situ data to infer thermophysical properties enables the environmental conditions the envelope is exposed to and its state of conservation, such as moisture accumulation, to be accounted for [8,12]. In situ measurement also facilitates the quality assessment of building construction and the assessment of the performance of building elements where the material properties and stratigraphy are not certain [13,14]. The impact of inhomogeneities in the structure, such as delamination and cracks [12,15], poor detailing, layout and/or workmanship [8,15], and thermal bridges [12] may also be better understood with in situ measurements.

In addition to contributing to the performance gap, the use of unrepresentative thermophysical characteristics may affect the proposed heating strategy of a building, the cost-effectiveness of energy-saving measures and the implementation of appropriate retrofitting strategies. Consequently, the evaluation of the actual thermophysical properties of the building stock from monitored data is widely considered advantageous compared to the use of tabulated data [16] both to minimise the performance gap and to improve the overall quality of the building process by feeding back the learnings into the system.

In situ measurements have been widely used in industry and academia to estimate the thermophysical properties of building elements [17–20]. However, the cost, time and expertise required

* Corresponding author.
E-mail address: virginia.gori.12@ucl.ac.uk (V. Gori).

http://dx.doi.org/10.1016/j.enbuild.2016.10.043

Nomenclature

T_{int}, T_{ext} measured internal and external surface temperature (°C)
$T^{0}_{C_n}$ initial temperature of the nth lumped thermal mass (°C)
$Q_{\mathrm{m,in}}$, $Q_{\mathrm{m,out}}$ measured heat flux into and out of the internal and external surfaces ($\mathrm{Wm^{-2}}$)
$Q_{\mathrm{e,in}}$, $Q_{\mathrm{e,out}}$ estimated heat flux into and out of the internal and external surfaces ($\mathrm{Wm^{-2}}$)
S complex Laplace variable representing the derivative operator
Z time-shift operator
τ sampling interval (*i.e.* the interval between measurements) (s)
R_n n-th lumped thermal resistance (starting from the internal side) ($\mathrm{m^2KW^{-1}}$)
C_n n-th lumped thermal mass (starting from the internal side) ($\mathrm{Jm^{-2}K^{-1}}$)
T_{C_n} estimated temperature of the nth lumped thermal mass (°C)
θ vector of the unknown parameters of the model
$\mathrm{P}(\theta|D, H)$ posterior probability distribution, given the data D and the model H
$\mathrm{P}(D|\theta, H)$ likelihood
$\mathrm{P}(\theta|H)$ prior probability distribution
$\mathrm{P}(D|H)$ evidence
ΔL_j width of the uniform prior probability of the jth parameter
$\Phi_{\mathrm{e},\varepsilon}$, $\Phi_{\mathrm{m},\varepsilon}$ estimated and observed time series for the data stream ε
$\sigma_{\Phi,\varepsilon}$ standard deviation of a noise term affecting the measurements
$\delta^{\mathrm{r}}_{\Phi,\varepsilon}$, $\delta^{\mathrm{a}}_{\Phi,\varepsilon}$ relative and absolute uncertainty affecting the measurements
$\chi^2_{\varepsilon}(\theta, H)$ Chi-squared function for the data stream ε
A inverse of the Hessian of the negative logarithm of the posterior at MAP

Superscripts
p, $p-1$ current and previous time step

Subscripts
1TM single thermal mass model
2TM two thermal mass model
MAP maximum a posteriori estimation

to undertake high-quality in situ measurement and analysis is a barrier to the wider adoption of this method [21]. Several methods have been developed to estimate the thermophysical properties of buildings from monitoring campaigns (*e.g.*, [16,22–25]). The choice of method is generally dictated by the final purpose of the analysis, the available data, and the experience and expertise of the team; none of these methods can be considered the best in absolute terms [22]. The analysis may be undertaken by white-box methods, using models derived from first principles, or by inverse (or data-driven) methods matching our understanding of the system (*i.e.* the model) to the measured data using black- or grey-box models [26]. Black-box methods use statistical techniques to infer the relationships amongst the inputs and outputs and do not require any knowledge of the system; the parameters of the model do not have a direct physical interpretation [27]. Conversely, grey-box models combine the advantages of white- and black-box models by including physical knowledge in the statistical description of the system and its behaviour, using prior information of the relationships of its parameters [28], but can require the adoption of a large number of parameters.

This paper presents the development of a dynamic inverse grey-box method of estimating effective thermal mass, *U*-values and *R*-values, building on that presented in Biddulph et al. [13]. The method uses lumped thermal mass models to describe the heat transfer across the building element and Bayesian-based optimisation techniques to estimate the best set of model parameters, and includes detailed error analysis. This statistical framework provides the most probable value for the parameters, an estimate of their uncertainties, their probability distribution and correlations [13]. The method is non-destructive, in line with standard techniques [29], and requires limited knowledge about the materials and structure of the building element, which is essential for the robust study of different built forms where these parameters are often not well characterised.

The lumped thermal mass models adopted here enable the estimation of parameters with clear physical interpretation (*e.g.*, *R*-value and effective thermal mass), which can be subsequently used to gain useful insights into the thermophysical behaviour of the building and how this may be improved. Additionally, the short measurement campaigns required facilitate estimation of the response of the thermal properties of the building to changing conditions, such as wind and moisture. The use of interior and exterior heat flux measurements enable the inference of the thermal structure of the building element, and its response to heat flow out of and into the building. As such, the models are also scalable – more complex models may readily be implemented if corresponding data is available. Finally, this paper presents the use of Bayesian model comparison to select the model that best represents the recorded data. For this purpose we use the ratio of the evidences of the models tested [30, Chapter 28], which embodies the Occam's razor principle. The improved fit of more complicated models is offset against the increased prior space associated with the greater number of parameters. Unlike the likelihood ratio, this method does not require that the models tested are nested.

2. Case studies and monitoring campaign

Two solid walls of different construction have been studied using in situ monitoring and Bayesian statistical methods for the estimation of their thermophysical properties. The thermal resistance and mass of the two walls were explored by means of lumped thermal parameter models of different complexity, designed to provide a description of the heat transfer through the building element. Specifically, a single thermal mass model, as applied previously in [13] and now with an improved analysis method, and a two thermal mass model were implemented. The walls studied were expected to exhibit significantly different thermal performance: the first (OWall) was of brick construction and formed part of the external wall of an office building [50], whilst the second (TCWall) utilised aerated clay blocks and was located in a thermal chamber [51]. The two case studies and monitoring campaigns are discussed below.

2.1. Brick wall in an office building

The first case study (OWall) was a solid-brick wall located on the first floor above ground of an office building in central London (UK), oriented north-west-facing (327° between the normal to wall and north). The wall was 370 ± 7 mm thick, consisting of 20 ± 5 mm of plaster (expected to be lime) on the inside and 350 ± 5 mm of exposed solid brick masonry on the outside. The masonry depth

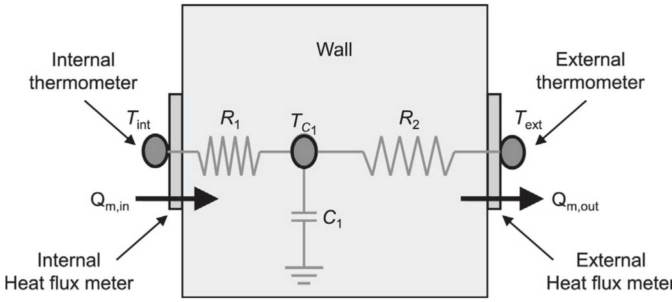

Fig. 1. Schematic diagram of the single thermal mass model (1TM) showing the equivalent electrical circuit for the heat transfer through the wall. Parameters of the model are: the effective thermal mass (C_1), its initial temperature $\left(T^0_{C_1}\right)$ and two thermal resistances (R_1, R_2). The measured quantities are: the internal (T_{int}) and external (T_{ext}) temperatures of the wall surface and the heat fluxes entering and leaving the wall from the internal $\left(Q_{m,in}\right)$ and external ($Q_{m,out}$) surfaces.

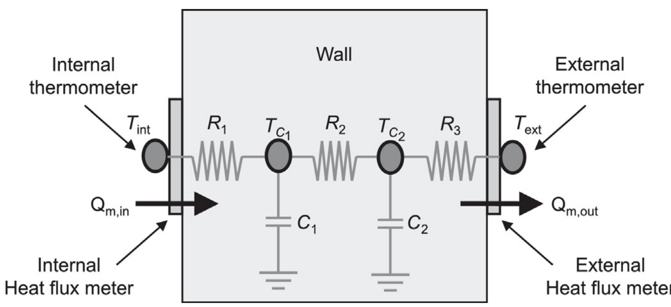

Fig. 2. Schematic diagram of the two thermal mass model (2TM) showing the equivalent electrical circuit for heat transfer through the wall. Parameters of the model are: the two effective thermal masses (C_1, C_2), their initial temperatures $\left(T^0_{C_1}, T^0_{C_2}\right)$ and three thermal resistances (R_1, R_2, R_3). The measured quantities are the internal (T_{int}) and external (T_{ext}) surface temperatures of the wall and the internal $\left(Q_{m,in}\right)$ and external ($Q_{m,out}$) heat flux through the wall.

was expected to comprise one and a half bricks, potentially with air gaps at the interface between adjacent bricks.

The OWall was instrumented (Figs. 1 and 2) with two Hukseflux HFP01 [31] heat flux plates (HFP) and two type-T thermocouples placed in-line with each other on opposite sides. The external HFP was secured using a water-resistant elastomeric polymer on the edge of the plate and thermal paste on the measuring area, while the internal one was fixed by covering the wall-facing side of the sensor with a layer of low-tack tape followed by a layer of double-sided tape [32]. Since the fixing layers are very thin, their additional thermal mass and resistance are assumed negligible in comparison to those of the wall [32]. The thermocouples were taped on top of each HFP (on the guard ring, outside the measuring area), using thermal paste to ensure thermal contact [32]. As the thermal resistance $\left(6.25 \times 10^{-3}\,\mathrm{m^{-2}K^{-1}W}\right)$ of the HFP [31] is about 1% of the typical resistance of a solid-brick wall similar to the OWall, the difference between the wall and HFP surface temperatures is assumed negligible. A Campbell Scientific CR1000 [33] data logger was used to record the data. Data were sampled every 5 s and averaged over 5 min intervals. For the purpose of this paper, the time series analysed was selected such that the difference between the internal and external temperatures was comparable to that used in the thermal chamber.

2.2. Aerated clay block wall in an environmental chamber

The second wall (TCWall) was built in the centre of a thermal chamber to minimise possible edge effects introduced by the structure of the chamber itself. The wall was subdivided into eight sections (1865 mm by 500 mm) to test different wall construction technologies [34]. The section investigated in this paper is a 303 ± 3 mm thick heavy-weight solid-wall constituted of seven layers. From the outside it comprised: 175 ± 2 mm of aerated clay blocks, 10 ± 2 mm of gypsum plaster, 5 ± 1 mm of lime plaster, 20 ± 1 mm of woodfibre insulation board, 0.10 ± 0.05 mm functional layer glued to a 80 ± 1 mm of woodfibre insulation board and 12.5 ± 0.5 mm of gypsum fibreboard. This section was chosen as it is of heavy-weight construction, similarly to the OWall, but it has significantly different structure and expected thermal mass distribution, providing a useful contrast to the OWall (Section 2.1).

The wall was instrumented (Figs. 1 and 2) with two Hukseflux HFP01 [31] HFP and two thermistors, mounted on the wall surface close to each HFP. The pairs of instruments were placed in-line with each other on opposite sides, similarly to the OWall. Duct tape was used to fix the HFP (measuring area excluded) and thermistors to the wall; a layer of thermal compound was applied under the sensors to ensure good thermal contact. A Campbell Scientific CR3000 [35] data logger was used to record the heat flux entering and leaving the wall, while an Eltek Squirrel [36] data logger was used to record surface temperatures. Data were averaged and recorded over 5 min intervals.

External ambient temperature profile in the thermal chamber was set to repeat hourly temperatures of a typical day derived from the UK Test Reference Year (TRY) for Manchester [37]. The indoor daily profile was set to replicate a typical UK indoor heating pattern derived from the Warm Front dataset, a project where air temperature and relative humidity were monitored for up to 4 weeks in the main living spaces of more than 1600 dwellings in five urban areas across the UK [38].

3. Theory and calculation

In this paper, two lumped thermal parameter models (Sections 3.1.1 and 3.1.2) were applied to describe the heat transfer through a building element. Firstly, model fitting was performed to estimate the best-fit parameters for each model (Section 3.2) and calculate the associated error matrix. Then, model selection was performed using the Bayesian odds ratio method (Section 3.3) [30, Chapter 28].

3.1. Thermal models of the wall

Two physically informed lumped thermal mass models were implemented to describe the walls in terms of thermophysical parameters, which are assumed to be constant during the monitoring period. Both models assume one-dimensional heat transfer perpendicular to the wall surfaces [29].

3.1.1. The single thermal mass model

The single thermal mass model (1TM) describes the heat flow through the wall using a physically informed equivalent electrical circuit constituted of two thermal resistances and a lumped thermal mass, as illustrated in Fig. 1. Heat may be stored by or released from the thermal mass, creating a time shift in the response of the measured heat flux to changes in external and internal temperature. This paper adopts an improved method for the discretisation of the single thermal mass model previously introduced in [13]. The backward difference transform (or rectangular rule) is replaced by the bilinear transform (or trapezoidal rule) which provides a better approximation to the derivative operation [39, Chapter 8.1.2].

The 1TM model (Fig. 1) incorporates four unknown parameters $\theta_{1TM} = \left[R_1, R_2, C_1, T^0_{C_1}\right]^T$ (*i.e.* respectively two thermal resistances, one effective thermal mass and its initial temperature). The temperature of the effective thermal mass $\left(T_{C_1}\right)$ is proportional to the heat stored in the effective thermal mass (C_1), which is in turn the integral of the net heat flux entering it. The temperature of the effective thermal mass can be estimated by electrical analogy to heat transfer and imposing the conservation of heat. The Laplace transform [40, Chapter 2.5] was used to replace the linear differential equations (necessary to describe the heat flux released by the effective thermal mass) with polynomial operations:

$$SC_1T_{C_1} = \frac{T_{int} - T_{C_1}}{R_1} + \frac{T_{ext} - T_{C_1}}{R_2}, \tag{1}$$

where T_{int} and T_{ext} are the internal and external temperature of the wall surface; S is the complex Laplace variable representing the derivative operator. This differential equation was approximated by a difference equation to sample the continuous-time system into discrete-time steps. The bilinear transform [39, Chapter 8.1.2] was used to approximate the derivative operator using the time-shift operator Z:

$$S = \frac{2\left(1 - Z^{-1}\right)}{\tau\left(1 + Z^{-1}\right)} \tag{2}$$

where 1 and Z^{-1} return the value of the signal at the current and previous time step, respectively; τ is the sampling interval (*i.e.* the interval between measurements). Substituting Eq. (2) into Eq. (1), rearranging and applying the time-shift operator, the temperature of the effective thermal mass at each time step can be estimated as:

$$T^p_{C_1} = \frac{\left(T^p_{int} + T^{p-1}_{int}\right)/R_1 + \left(T^p_{ext} + T^{p-1}_{ext}\right)/R_2 + \left(2C_1/\tau - 1/R_1 - 1/R_2\right)T^{p-1}_{C_1}}{2C_1/\tau + 1/R_1 + 1/R_2} \tag{3}$$

where $T^p_{C_1}$ and $T^{p-1}_{C_1}$ are respectively the temperature of the effective thermal mass at the current (p) and previous ($p-1$) time step; T^p_{int}, T^p_{ext} and T^{p-1}_{int}, T^{p-1}_{ext} are respectively the internal and external temperature of the wall surface at the current and previous time step. The estimated heat flow from the indoor ambient into the internal wall surface $\left(Q^p_{e,in}\right)$ and the estimated heat flow leaving the external surface of the wall $\left(Q^p_{e,out}\right)$ at each time step can be computed as:

$$Q^p_{e,in} = \frac{T^p_{int} - T^p_{C_1}}{R_1}; \quad Q^p_{e,out} = \frac{T^p_{C_1} - T^p_{ext}}{R_2}. \tag{4}$$

The model parameters θ_{1TM} can be estimated given the measured heat transfer from the inside $\left(Q^p_{m,in}\right)$ or the outside $\left(Q^p_{m,out}\right)$ surface of the wall or both simultaneously, as illustrated in Section 3.2.

3.1.2. The two thermal mass model

A more complex lumped thermal mass model, the two thermal mass (2TM) model (Fig. 2), was developed to describe the heat transfer through the wall. It includes seven parameters $\theta_{2TM} = \left[R_1, R_2, R_3, C_1, C_2, T^0_{C_1}, T^0_{C_2}\right]^T$ (*i.e.* respectively three thermal resistances, two effective thermal masses and their initial temperatures).

Adopting the same approach as described in Section 3.1.1, the temperature of the two effective thermal masses $\left(T_{C_1}, T_{C_2}\right)$ can be calculated by imposing the equilibrium of the heat flux at each node:

$$\begin{cases} SC_1T_{C_1} = \dfrac{T_{int} - T_{C_1}}{R_1} + \dfrac{T_{C_2} - T_{C_1}}{R_2} \\ SC_2T_{C_2} = \dfrac{T_{C_1} - T_{C_2}}{R_2} + \dfrac{T_{ext} - T_{C_2}}{R_3} \end{cases}. \tag{5}$$

Substituting the Laplace variable in Eq. (5) with the bilinear transform (Eq. (2)) and rearranging, the system of equations in Eq. (5) becomes:

$$\begin{cases} \left(\dfrac{2}{\tau}C_1 + \dfrac{1}{R_1} + \dfrac{1}{R_2}\right)T^p_{C_1} - \dfrac{1}{R_2}T^p_{C_2} = \left(\dfrac{2}{\tau}C_1 - \dfrac{1}{R_1} - \dfrac{1}{R_2}\right)T^{p-1}_{C_1} + \dfrac{1}{R_2}T^{p-1}_{C_2} + \dfrac{T^p_{int} + T^{p-1}_{int}}{R_1} \\ -\dfrac{1}{R_2}T^p_{C_1} + \left(\dfrac{2}{\tau}C_2 + \dfrac{1}{R_2} + \dfrac{1}{R_3}\right)T^p_{C_2} = \dfrac{1}{R_2}T^{p-1}_{C_1} + \left(\dfrac{2}{\tau}C_2 - \dfrac{1}{R_2} - \dfrac{1}{R_3}\right)T^{p-1}_{C_2} + \dfrac{T^p_{ext} + T^{p-1}_{ext}}{R_3} \end{cases} \tag{6}$$

where $T^p_{C_1}$, $T^p_{C_2}$ are the temperature of the two effective thermal masses at the current time step (p); $T^{p-1}_{C_1}$, $T^{p-1}_{C_2}$ are the temperature of the two effective thermal masses at the previous time step ($p-1$). For simplicity, the coefficients of the parameters and the constant terms are renamed as follows:

$$a_{11} = \frac{2}{\tau}C_1 + \frac{1}{R_1} + \frac{1}{R_2} \tag{7a}$$

$$a_{12} = -\frac{1}{R_2} \tag{7b}$$

$$a_{13} = \left(\frac{2}{\tau}C_1 - \frac{1}{R_1} - \frac{1}{R_2}\right)T^{p-1}_{C_1} + \frac{1}{R_2}T^{p-1}_{C_2} + \frac{T^p_{int} + T^{p-1}_{int}}{R_1} \tag{7c}$$

$$a_{21} = -\frac{1}{R_2} \tag{7d}$$

$$a_{22} = \frac{2}{\tau}C_2 + \frac{1}{R_2} + \frac{1}{R_3} \tag{7e}$$

$$a_{23} = \frac{1}{R_2}T^{p-1}_{C_1} + \left(\frac{2}{\tau}C_2 - \frac{1}{R_2} - \frac{1}{R_3}\right)T^{p-1}_{C_2} + \frac{T^p_{ext} + T^{p-1}_{ext}}{R_3}. \tag{7f}$$

The temperature of the two effective thermal masses at each time step $\left(T^p_{C_1}, T^p_{C_2}\right)$ can be estimated from Eq. (6) as:

$$T^p_{C_1} = \frac{a_{13} - a_{12}T^p_{C_2}}{a_{11}}; \quad T^p_{C_2} = \frac{a_{11}a_{23} - a_{21}a_{13}}{a_{22}a_{11} - a_{21}a_{12}}. \tag{8}$$

Finally, the estimated heat flux entering the indoor surface $\left(Q^p_{e,in}\right)$ and leaving the external surface $\left(Q^p_{e,out}\right)$ of the wall at each time step can be calculated as:

$$Q^p_{e,in} = \frac{T^p_{int} - T^p_{C_1}}{R_1}; \quad Q^p_{e,out} = \frac{T^p_{C_2} - T^p_{ext}}{R_3}. \tag{9}$$

The model parameters θ_{2TM} can be estimated given the measured heat transfer from the inside $\left(Q^p_{m,in}\right)$ and the outside $\left(Q^p_{m,out}\right)$ surface of the wall, as described in Section 3.2.

3.2. Model fitting and best-fit parameter estimation

The 1TM and 2TM models (Section 3.1) utilise parameters that describe the thermophysical characteristics of the structure and the heat transfer across it. For each model ($H \in \{H_{1TM}, H_{2TM}\}$), we chose as best-fit parameters $\left(\theta_{MAP}\right)$ the maximum a posteriori

(MAP) estimates[1] [30]. Adopting a Bayesian approach [42], the posterior probability (*i.e.* the probability of the parameters θ, given the data D) can be rewritten as the product of the prior probability (*i.e.* the initial estimated probability distribution of the parameters of the model) and the likelihood (*i.e.* a data-dependent term describing the probability of obtaining the measured data given the model adopted and its parameters) divided by the evidence (*i.e.* a normalisation factor). This yields:

$$\theta_{\mathrm{MAP}} = \arg\max_{\theta} \mathrm{P}\left(\theta \middle| D, H\right) = \arg\max_{\theta} \frac{\mathrm{P}\left(D \middle| \theta, H\right) \mathrm{P}\left(\theta \middle| H\right)}{\mathrm{P}\left(D \middle| H\right)} \tag{10}$$

where $\mathrm{P}\left(\theta \middle| D, H\right)$ is the posterior probability; $\mathrm{P}\left(D \middle| \theta, H\right)$ is the likelihood; $\mathrm{P}\left(\theta \middle| H\right)$ is the prior probability; $\mathrm{P}\left(D \middle| H\right)$ is the evidence. In this analysis error in the dependent variables (model outputs) is accounted for through an additive noise term including all quantifiable sources of uncertainties (*e.g.*, errors on the observed quantities both in the minimisation and parameter estimation processes, fitting errors and errors on the outputs). The additive noise term is defined a priori to account for all the known sources of uncertainties affecting the observed data. Assuming that the observation errors are Gaussian-distributed and that the residuals between the estimations and the measurements are independent at each time step, the likelihood can be computed as:

$$\mathrm{P}\left(D \middle| \theta, H\right) = \prod_{\varepsilon \in E} \prod_{p=1}^{n} \frac{1}{\sigma_{\Phi,\varepsilon}\sqrt{2\pi}} \exp\left[-\frac{\left(\Phi^{p}_{\mathrm{e},\varepsilon} - \Phi^{p}_{\mathrm{m},\varepsilon}\right)^2}{2\sigma^2_{\Phi,\varepsilon}}\right] \tag{11}$$

where E is the set of data streams ε contributing to the fit (in this application E coincides with the set of HFPs analysed and ε can be either the internal or external one); p is the index of the time step and n the number of observations per data stream; $\sigma_{\Phi,\varepsilon}$ is the standard deviation of an additive noise term affecting each measured data stream (the heat flux in this case; see Section 4.2.1); $\Phi^{p}_{\mathrm{e},\varepsilon}$ and $\Phi^{p}_{\mathrm{m},\varepsilon}$ are respectively the estimated and observed data stream at each time step (in this paper $\Phi^{p}_{\mathrm{e},\varepsilon} \in \left\{Q^{p}_{\mathrm{e,in}}, Q^{p}_{\mathrm{e,out}}\right\}$ and $\Phi^{p}_{\mathrm{m},\varepsilon} \in \left\{Q^{p}_{\mathrm{m,in}}, Q^{p}_{\mathrm{m,out}}\right\}$). Taking the natural logarithm of Eq. (10), the best-fit parameters can be estimated as:

$$\begin{aligned}
\theta_{\mathrm{MAP}} &= \arg\max_{\theta} \ln \mathrm{P}\left(D \middle| \theta, H\right) + \ln \mathrm{P}\left(\theta \middle| H\right) \\
&= \arg\min_{\theta} \sum_{\varepsilon \in E} \sum_{p=1}^{n} \frac{\left(\Phi^{p}_{\mathrm{e},\varepsilon} - \Phi^{p}_{\mathrm{m},\varepsilon}\right)^2}{2\sigma^2_{\Phi,\varepsilon}} - \ln \mathrm{P}\left(\theta \middle| H\right) \\
&= \arg\min_{\theta} \chi^2_{\varepsilon}\left(\theta, H\right) - \ln \mathrm{P}\left(\theta \middle| H\right)
\end{aligned} \tag{12}$$

where $\chi^2_{\varepsilon}\left(\theta, H\right)$ is a chi-squared function representing the residuals between the measured and estimated quantities for each data stream. A numerical minimisation software (the Scipy implementation of the basinhopping algorithm using the Powell method) is used to identify the global minimum of the posterior probability surface and calculate the error matrix from the matrix of the Hessian around it [43].

For the 1TM model, the chi-squared function can be calculated from the internal measured heat flux only $\chi^2_{\mathrm{in}} = \frac{1}{\sigma^2_{\Phi,\mathrm{in}}} \sum_p \left(Q^{p}_{\mathrm{e,in}} - Q^{p}_{\mathrm{m,in}}\right)^2$ (as in [13]), the external heat flux only $\chi^2_{\mathrm{out}} = \frac{1}{\sigma^2_{\Phi,\mathrm{out}}} \sum_p \left(Q^{p}_{\mathrm{e,out}} - Q^{p}_{\mathrm{m,out}}\right)^2$ or both of them simultaneously $\chi^2 = \chi^2_{\mathrm{in}} + \chi^2_{\mathrm{out}}$. The latter is used for the 2TM model and the 1TM model when both the internal and external heat fluxes are used in the optimisation process.

[1] Analysis of the full posterior probability of the parameters by means of a Markov Chain Monte Carlo (MCMC) approach may provide supplementary insight and is the topic of ongoing research by the authors [41].

3.3. Model selection

The two models (1TM and 2TM) have different complexity, in this case represented by the number of parameters. In general, more complex models result in a better fit to the training data, which is in principle desirable. However, if the model is too complex it starts to describe the noise in the observations instead of the underlying process – a phenomenon known as overfitting [30, Chapters 39,44]. Bayesian model comparison accounts for this issue by requiring an improved goodness of fit as the number of parameters increases because increasing the number of parameters enlarges the prior probability space, effectively penalising more complicated models [44–46]. Therefore, the plausibility of two different models ($H_{\mathrm{1TM}}, H_{\mathrm{2TM}}$) fitted to their most probable parameters $\left(\theta_{\mathrm{MAP1}}, \theta_{\mathrm{MAP2}}\right)$ can be inferred using the ratio of their posterior probability (odds ratio) [30, Chapter 28]:

$$\frac{\mathrm{P}\left(H_{\mathrm{1TM}} \middle| D\right)}{\mathrm{P}\left(H_{\mathrm{2TM}} \middle| D\right)} = \frac{\mathrm{P}\left(D \middle| H_{\mathrm{1TM}}\right) \mathrm{P}(H_{\mathrm{1TM}})}{\mathrm{P}\left(D \middle| H_{\mathrm{2TM}}\right) \mathrm{P}(H_{\mathrm{2TM}})}, \tag{13}$$

where $\mathrm{P}\left(H_{\mathrm{1TM}} \middle| D\right)$, $\mathrm{P}\left(H_{\mathrm{2TM}} \middle| D\right)$ are the posterior probability of each model; $\mathrm{P}\left(D \middle| H_{\mathrm{1TM}}\right)$, $\mathrm{P}\left(D \middle| H_{\mathrm{2TM}}\right)$ are the evidences; $\mathrm{P}(H_{\mathrm{1TM}})$, $\mathrm{P}(H_{\mathrm{2TM}})$ are the prior probabilities.

For each model H, the evidence (or marginal likelihood) can be calculated by marginalising over the parameters θ:

$$\mathrm{P}\left(D \middle| H\right) = \int \mathrm{P}\left(D, \theta \middle| H\right) d\theta = \int \mathrm{P}\left(D \middle| \theta, H\right) \mathrm{P}\left(\theta \middle| H\right) d\theta \tag{14}$$

where $\mathrm{P}\left(D, \theta \middle| H\right)$ is the joint probability of the data and the parameters given the model; $\mathrm{P}\left(D \middle| \theta, H\right)$ is the likelihood and $\mathrm{P}\left(\theta \middle| H\right)$ is the prior probability of the parameters. Assuming that the posterior distribution can be approximated with a Gaussian distribution centered at the most probable value of the parameters given the data $\left(\theta_{\mathrm{MAP}}\right)$, the Laplace method can be used to approximate Eq. (14) [30, Chapter 28]:

$$\mathrm{P}\left(D \middle| H\right) \approx \mathrm{P}\left(D \middle| \theta_{\mathrm{MAP}}, H\right) \mathrm{P}\left(\theta_{\mathrm{MAP}} \middle| H\right) \left[\det(2\pi A)\right]^{1/2} \tag{15}$$

where $\mathrm{P}\left(D \middle| \theta_{\mathrm{MAP}}, H\right)$ is the best-fit likelihood; $\mathrm{P}\left(\theta_{\mathrm{MAP}} \middle| H\right) \left[\det(2\pi A)\right]^{1/2}$ is the Occam's factor; $\mathrm{P}\left(\theta_{\mathrm{MAP}} \middle| H\right)$, $\left[\det(2\pi A)\right]^{1/2}$ are respectively the prior probability and a coefficient that depends on the curvature of the posterior distribution around the best-fit parameters; A is the inverse of the Hessian of the negative logarithm of the posterior probability distribution computed at the MAP and corresponds to the covariance matrix under the Gaussian approximation. The best-fit likelihood $\mathrm{P}\left(D \middle| \theta_{\mathrm{MAP}}, H\right)$ can be obtained computing Eq. (11) for $\theta = \theta_{\mathrm{MAP}}$.

The prior probability distribution of the parameters of the model is calculated as the product of the probability density functions associated with each parameter. If uniform priors are adopted, as here, $\mathrm{P}\left(\theta_{\mathrm{MAP}} \middle| H\right)$ is calculated as:

$$\mathrm{P}\left(\theta_{\mathrm{MAP}} \middle| H\right) = \prod_{j=1}^{z} \left(\Delta L_j\right)^{-1} \tag{16}$$

where z is the number of parameters of the model and ΔL_j is the width of the uniform prior probability of each parameter j. Therefore, for each model the evidence $\mathrm{P}\left(D \middle| H\right)$ can be calculated according to Eq. (15) as:

$$\mathrm{P}\left(D\middle|H\right) = \left[\prod_{\varepsilon\in E}\prod_{p=1}^{n}\frac{1}{\sigma_{\Phi,\varepsilon}\sqrt{2\pi}}\exp\left(-\frac{\left(\Phi^{p}_{e,\varepsilon}-\Phi^{p}_{m,\varepsilon}\right)^{2}}{2\sigma^{2}_{\Phi,\varepsilon}}\right)\right] \times\left[\prod_{j=1}^{z}\left(\Delta L_j\right)^{-1}\right]\left[\det\left(2\pi A\right)\right]^{1/2}. \tag{17}$$

To provide a fair comparison of the performance of the models, the same information (*i.e.* number of data streams and observations) has to be used for the optimisation of each model. In this paper the model selection has been performed comparing the 2TM model with the 1TM model fitted using both the indoor and external heat flux measurements (Section 3.2). Thus, both models used four measured inputs, namely the indoor and external heat fluxes and temperatures. Additionally, the same time series was used to fit the two models and to estimate the most probable thermophysical parameters.

3.4. Prior probability distribution

Estimates of the *R*-value (and *U*-value) and total thermal mass of the walls are available by calculation using the dimension of each layer and the tabulated thermophysical properties of each material (Section 4.1). However, the values calculated from tabulated thermophysical properties may not be representative of the actual thermal performance of the case studies investigated as the specific materials, structure and condition of the wall (*e.g.*, moisture content) are unknown. Consequently, large non-informative uniform priors were used in this application for the estimation of the parameters to capture potential unexpected performances due to limited knowledge of the walls. Conversely, non-uniform prior (*e.g.*, log-normal distributed) can be adopted if more information about the geometry and the distribution of the thermophysical properties of the building materials are available [41].

Appropriate and consistent prior information is important for parameter estimation, but it is crucial for model comparison. Therefore the bounds on all resistances in both models is set to the same range of 0 to 4 $W^{-1}m^2K$, all effective thermal masses 0 to 2,000,000 $Jm^{-2}K^{-1}$ and initial temperatures of the effective thermal masses from −5 to 30°C. These ranges encompass all expected values, with an ample safety margin.

4. Results and discussion

The thermophysical properties of the two walls were estimated using the steady-state average method (AM) [29] and the dynamic lumped thermal parameter models, with one (1TM) and two thermal masses (2TM). *U*-values were also calculated using thermophysical properties from look up tables published in the literature, on the basis of the wall structure. For each case study, the model selection was performed to assess which model is the best to describe the observed data.

4.1. Literature thermophysical properties

An *U*-value of 0.35 $Wm^{-2}K^{-1}$ was obtained for the TCWall from the tabulated thermophysical properties of the different components (Section 2.2) provided by the manufacturers. For the OWall, a range of possible *U*-values was defined because of the lack of specific information on the density and characteristics of its materials (Section 2.1). According to the Chartered Institute of Building Services Engineers (CIBSE) Environmental Design – Guide A [47], the thermal conductivity of solid bricks is expected to be in the range 0.50 to 1.31 mKW^{-1}, while lime plaster ranges between 0.70 and 0.80 mKW^{-1}. Mortar joints between bricks were not accounted for separately (*i.e.* the brick layer was considered homogeneous) in the calculation as the thermal conductivity of mortar is within the thermal conductivity range for solid brick. On this basis, the *U*-value of the OWall is expected to be in the range of 1.11 to 2.16 $Wm^{-2}K^{-1}$, obtained by combining the upper and lower values of thermal conductivity of the materials constituting the wall. In both cases, constant indoor $\left(R_{s\,in} = 0.13\,m^2KW^{-1}\right)$ and external $\left(R_{s\,out} = 0.04\,m^2KW^{-1}\right)$ air film resistances [48] were used in the *U*-value calculation.

The total thermal mass of each wall was computed using values of density and specific heat capacity from [47] for the OWall and from manufacturers' specifications for the TCWall. The computed total thermal mass ranged between 379,700 and 697,400 $Jm^{-2}K^{-1}$ for the former case study, while it resulted in a value of 274,800 $Jm^{-2}K^{-1}$ for the latter. In addition to the total thermal mass, the thermal masses as seen from the internal and external ambient were computed following the simplified method for the calculation of heat capacity described in Appendix A of the EN ISO 13786 standard [49]. For the OWall, this yields an internal thermal mass ranging between 107,500 and 180,100 $Jm^{-2}K^{-1}$ and an external one in the range 100,800 to 191,600 $Jm^{-2}K^{-1}$. Similarly, the simplified method predicts an internal thermal mass of 48,000 $Jm^{-2}K^{-1}$ and an external one of 119,000 $Jm^{-2}K^{-1}$ for the TCWall.

The wide ranges of potential *U*-values and thermal masses of the OWall highlight the difficulties often associated with the calculation of representative values from tabulated thermophysical properties, especially when inaccurate or insufficient information about the building are available. Very often only visual inspections or quick surveys are possible, leading to potential difficulties in identifying different building layers, measuring their thicknesses, or identifying similarly looking materials and inferring their properties from look up tables in the literature. Tabulated values may present quite broad ranges even for a single material and they do not account for the issues associated with in situ performance, such as moisture content or changing environmental conditions.

4.2. Estimation of the thermophysical properties from in situ measurements

The results of the analysis of the measured data for the OWall and TCWall are presented below, preceded by details of the error estimation. For each case study, the criteria set out in the BS ISO 9869-1 standard [29, p.9] were imposed to determine the number of full days required by the AM to return a valid estimation of the *R*- and *U*-value of the wall. The time series so obtained was also used to estimate the thermophysical parameters with the 1TM and 2TM models. For each method, the total *R*-value (and *U*-value) was calculated as the surface-to-surface thermal resistance plus a correction factor. The latter accounts for the constant indoor and external air film resistances introduced in Section 4.1 and removes the thermal resistance of the HFPs [31]. For the 1TM and 2TM models, the surface-to-surface R-value was calculated as the sum of the individual thermal resistance estimates returned by the analysis.

4.2.1. Estimation of the uncertainties

4.2.1.1. Estimation of the standard deviation of the additive noise term affecting the measured heat flux. For each HFP involved in the analysis, the standard deviation of the additive noise term $\sigma_{\Phi,\varepsilon}$ affecting the measured heat flux has to account for all the quantifiable sources of uncertainties affecting the observations (Sections 3.2 and 3.3). Assuming that, in line with expectations, each source of uncertainty is independent, the total relative and absolute uncertainty $\left(\delta^{r}_{\Phi,\varepsilon}, \delta^{a}_{\Phi,\varepsilon}\right)$ affecting the measurements of each HFP was calculated as the quadrature sum of the following uncertainties: (a) the accuracy of the equipment (*i.e.* HFP and data logging system(s) involved in the analysis); (b) the effect of random variations caused by imperfect thermal contact between the sensor and the wall (5% according to [29, p.13]); and (c) an uncertainty due to the modification of the isotherms caused by the presence of the HFP (3% according to [29, p.13]). The variance of the additive noise term of each measured heat flux was then calculated as:

$$\sigma^2_{\Phi,\varepsilon} = \left(\delta^{a}_{\Phi,\varepsilon}\right)^2 + \left(\frac{\sum_{p=1}^{n}\left|Q^{p}_{m,\varepsilon}\right|}{n}\delta^{r}_{\Phi,\varepsilon}\right)^2 \tag{18}$$

where $Q^{p}_{m,\varepsilon}$ is the measured heat flux at each recording interval (p) for each HFP (ε) used in the analysis (*i.e.* parameter estimation or model comparison).

4.2.1.2. Estimation of the systematic uncertainties on the U*-value.* For the AM, the total systematic uncertainty affecting the U-value was calculated through a first-order Taylor series expansion of its definition as function of heat flux and temperature difference. It included the quadrature sum of the total relative uncertainty on the measured heat flux as described in Section 4.2.1.1, the accuracy of the equipment used for temperature measurement (*i.e.* thermometers and data logging system(s)), and an extra 10% uncertainty that accounts for errors caused by the variations over time of the temperatures and heat flow, as suggested in [29, p.13]. Owing to the use of surface temperatures, the calculation omitted the 5% uncertainty suggested in [29, p.13] to account for the temperature variations within the space and the differences between air and radiant temperatures. For the dynamic method, the systematic error associated with the U-value was calculated indirectly from the derivative of the gradient of the posterior probability distribution at its maximum with respect to all the parameters and the systematic uncertainty contributing to the U-value estimation [41].

For the OWall, the relative systematic uncertainty on the U-value was 19% for the AM, 16% for the 1TM model (either using only the internal or both heat flux measurements) and 15% for the 2TM model. For the TCWall the relative systematic uncertainty was 15% for the AM, 11% for the 1TM model when using the internal heat flux only and 10% both for the 1TM model using both heat flux information and the 2TM model.

4.2.1.3. Estimation of the statistical uncertainties on the U*-value.* Statistical uncertainties on the 1TM and 2TM parameter estimates and its covariance matrix were estimated during Bayesian analysis. The statistical uncertainty on the U-value was calculated from the covariance matrix by applying a first-order Taylor series expansion of the definition of a U-value given the thermal resistances contributing to it. It is worth noting that in our case studies these uncertainties are small (the order of magnitude was 10^{-3} independently of the model optimised) and the total uncertainty is dominated by the systematic uncertainties because the number of parameters of the models is much less than the number of observations in the time series analysed. Statistical uncertainties are therefore omitted when presenting U-values, unless clearly stated.

4.2.2. Estimation of the thermophysical properties of the office wall

According to the criteria in [29, p.9] (see also Section 4.2), a three full-day time series (from the 5th to the 8th of October 2014) was analysed for the OWall. The surface-to-surface R-value calculated using the AM was 0.37 ± 0.07 m^2KW^{-1}, which resulted in a U-value of 1.89 ± 0.36 $Wm^{-2}K^{-1}$ after applying the correction factor described in Section 4.2.

The chi-squared function representing the likelihood for the 1TM model can be calculated in a number of ways to estimate the thermophysical properties of a wall (Section 3.2). One method, as previously presented in [13], is to use only the heat flux transferring through the interior surface of the wall (1 HF). As expected there is a reasonable match between the predicted[2] and measured interior heat flux (Fig. 3) but a poor fit when predicting the heat transferring through the exterior surface of the wall investigated; the estimates of the U-value was 1.73 ± 0.27 $Wm^{-2}K^{-1}$. A second way to calculate the chi-squared function for the 1TM model is to use both the interior and exterior heat flux measurements (2 HF); this produced a U-value estimate of 1.82 ± 0.30 $Wm^{-2}K^{-1}$. The heat fluxes estimated by the 1TM model when using both the measured interior and exterior heat fluxes are shown in Fig. 3; the prediction of the external heat flux is improved, to the detriment of the fit to the internal heat flux. The 2TM model requires both the interior and exterior heat flux measurements and returned a U-value of 1.71 ± 0.26 $Wm^{-2}K^{-1}$. The bottom panel of Fig. 3 illustrates the estimated and measured heat fluxes through the wall using the 2TM model. In this case there is good agreement both for the interior and exterior heat flux (Fig. 3 only shows a two-day period for illustrative and readability purposes, however the fitting performance shown is representative of the whole data set and of the TCWall case study). The model comparison is discussed in Section 4.3.

Estimates of the parameter values for all models are shown in Table 1. The estimates of the 2TM effective thermal masses $\left(C_1 = 212,900 \pm 1,800\,\mathrm{Jm^{-2}K^{-1}};\, C_2 = 113,100 \pm 1,000\,\mathrm{Jm^{-2}K^{-1}}\right)$ are comparable with those calculated from look up tables $\left(C_{int} = [107,500;\ 180,100]\,\mathrm{Jm^{-2}K^{-1}};\, C_{ext} = [100,800;\ 191,600]\,\mathrm{Jm^{-2}K^{-1}}\right)$ and shown in Section 4.1. Fig. 4 illustrates the estimates of the thermophysical properties of the wall using the AM, 1TM (both using 1 HF or 2 HF) and 2TM models for the OWall. It also highlights the wide range of possible R-values using tabulated properties due to uncertainty regarding the performance of the materials constituting the wall.

The measured interior and exterior surface temperatures, together with the estimated effective thermal mass temperatures in the 2TM model are shown in Fig. 5. As expected, both effective thermal mass temperatures respond to changes in surface temperature, out of phase with each other and the surface temperatures. As illustrated in Fig. 5 the temperature of the effective thermal mass closest to the exterior surface $\left(T_{C_2}\right)$ is sometimes lower than the surface temperature, indicating periods when the heat flow has reversed to be from the exterior into the wall.

4.2.3. Estimation of the thermophysical properties of the wall in the thermal chamber

Three full days of data were required for the TCWall to meet the criteria outlined in [29, p.9] (see also Section 4.2). Repeating the analysis described in Section 4.2.2, the adjusted U-value was 0.34 ± 0.05 $Wm^{-2}K^{-1}$ for the AM, 0.33 ± 0.04 $Wm^{-2}K^{-1}$ for the 1TM model using only the interior heat flux to calculate the chi-squared function, 0.33 ± 0.03 $Wm^{-2}K^{-1}$ for the 1TM model using both heat fluxes and 0.33 ± 0.03 $Wm^{-2}K^{-1}$ for the 2TM model. Estimates of the parameters for all models are shown in Table 2. Notably, the 2TM estimates of the two effective thermal masses $\left(C_1 = 46,700 \pm 500\,\mathrm{Jm^{-2}K^{-1}};\, C_2 = 119,100 \pm 800\,\mathrm{Jm^{-2}K^{-1}}\right)$ are in close agreement with those calculated from tabulated data $\left(C_{int} = 48,000\,\mathrm{Jm^{-2}K^{-1}};\, C_{ext} = 119,000\,\mathrm{Jm^{-2}K^{-1}}\right)$ and reported in Section 4.1. The predicted heat flows and temperatures of the thermal masses had comparable trends to those for the OWall.

Similarly to Fig. 4, a summary of the thermophysical properties obtained from all methods is shown in Fig. 6. The total thermal

[2] In this paper the term *predicted* is used in its statistical meaning of estimating the value of a random variable rather than as synonym of forecast, which implies making a prediction of the value of the variable at a given time in the future.

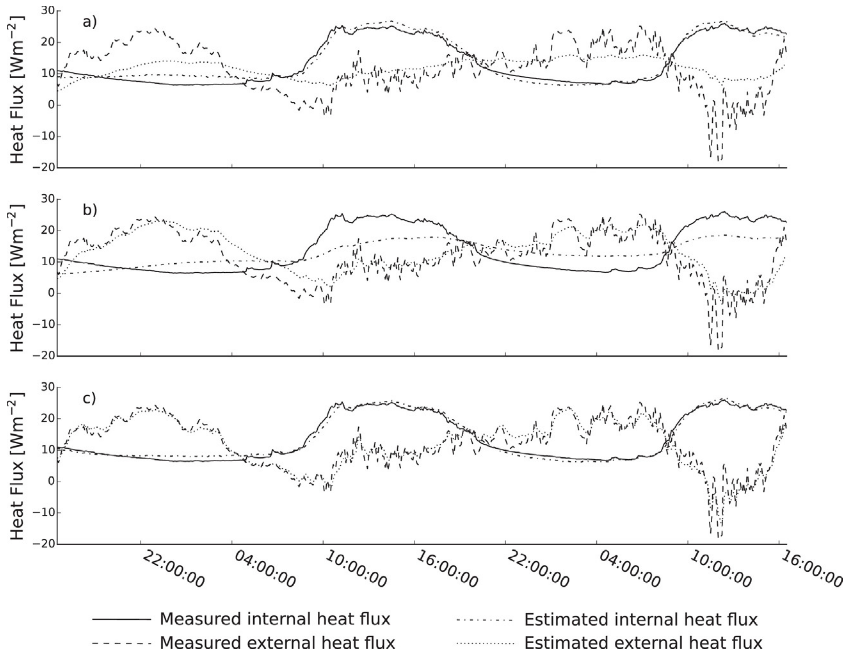

Fig. 3. Measured and estimated heat flows through the OWall by: (a) the 1TM model utilising data from the internal HFP; (b) the 1TM utilising both interior and exterior HFP and (c) the 2TM using both HFP.

Table 1
Thermophysical parameters estimated for the OWall. Only statistical errors from the model fitting are quoted; the number of significant figures was chosen to illustrate the level of statistical error.

Parameters	AM	1TM (1 HF)	1TM (2 HF)	2TM	Units
R_1	0.372	0.068 ± 0.001	0.248 ± 0.001	0.076 ± 0.001	m^2KW^{-1}
R_2		0.354 ± 0.002	0.145 ± 0.001	0.272 ± 0.001	m^2KW^{-1}
R_3				0.078 ± 0.001	m^2KW^{-1}
C_1		$224{,}900 \pm 1,600$	$269{,}600 \pm 2,500$	$212{,}900 \pm 1,800$	$Jm^{-2}K^{-1}$
C_2				$113{,}100 \pm 1,000$	$Jm^{-2}K^{-1}$
$T^0_{C_1}$		16.31 ± 0.02	15.37 ± 0.03	16.11 ± 0.02	$^\circ C$
$T^0_{C_2}$				15.27 ± 0.03	$^\circ C$
U-Value	1.868	1.708 ± 0.008	1.816 ± 0.005	1.713 ± 0.005	$Wm^{-2}K^{-1}$

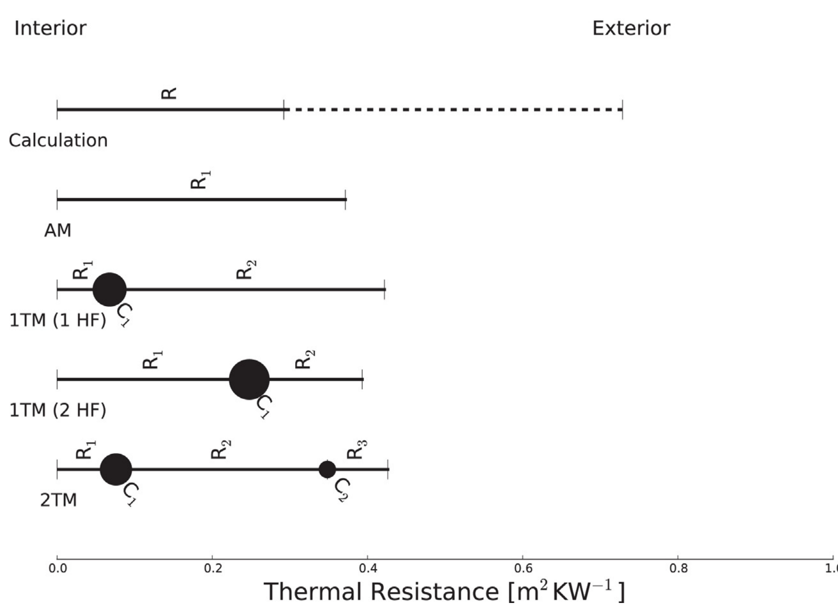

Fig. 4. Summary of the surface-to-surface R-value and size of the effective thermal mass(es) of the OWall as estimated with the AM and the dynamic method, with the 1TM (both using only the internal heat flux (1 HF) or both (2 HF)) and the 2TM models. The effective thermal mass is indicated by a solid circle with radius proportional to its magnitude. The expected range for the R-value calculated from the literature is also shown.

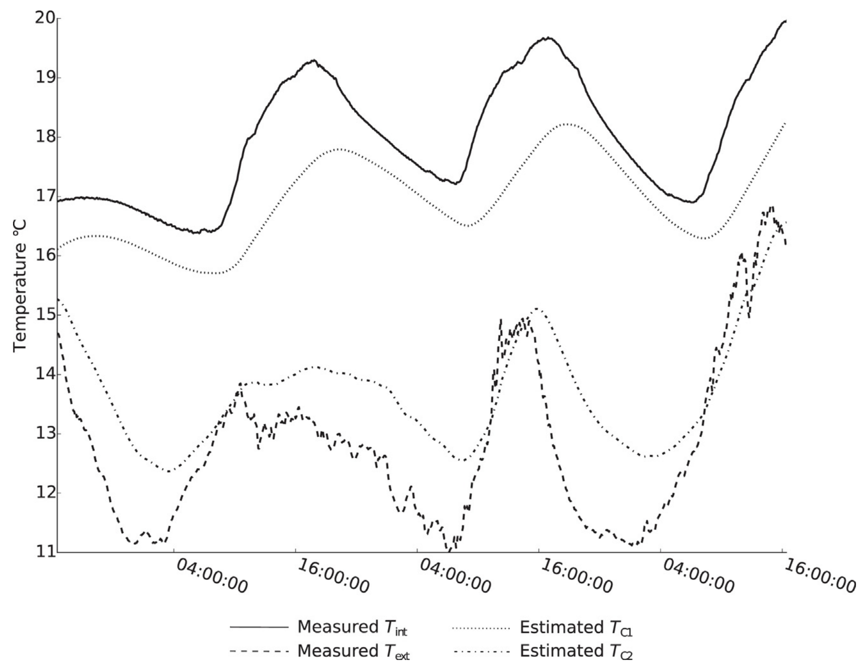

Fig. 5. Measured temperatures of the interior (T_{int}) and exterior (T_{ext}) wall surfaces and estimated temperatures of the first (T_{C_1}, closer to the interior surface) and second (T_{C_2}, closer to the exterior surface) effective thermal mass using the 2TM model for the OWall.

Table 2
Thermophysical parameters for the TCWall. Only statistical errors from the model fitting are quoted; the number of significant figures was chosen to illustrate the level of statistical error.

Parameters	AM	1TM (1 HF)	1TM (2 HF)	2TM	Units
R_1	2.790	0.256 ± 0.002	2.582 ± 0.010	0.287 ± 0.003	m^2KW^{-1}
R_2		2.600 ± 0.012	0.259 ± 0.001	2.365 ± 0.012	m^2KW^{-1}
R_3				0.249 ± 0.001	m^2KW^{-1}
C_1		$71,300 \pm 500$	$142,900 \pm 1,000$	$46,700 \pm 500$	$Jm^{-2}K^{-1}$
C_2				$119,100 \pm 800$	$Jm^{-2}K^{-1}$
$T^0_{C_1}$		18.86 ± 0.01	14.92 ± 0.02	18.85 ± 0.01	°C
$T^0_{C_2}$				14.83 ± 0.02	°C
U-Value	0.339	0.331 ± 0.001	0.333 ± 0.001	0.327 ± 0.001	$Wm^{-2}K^{-1}$

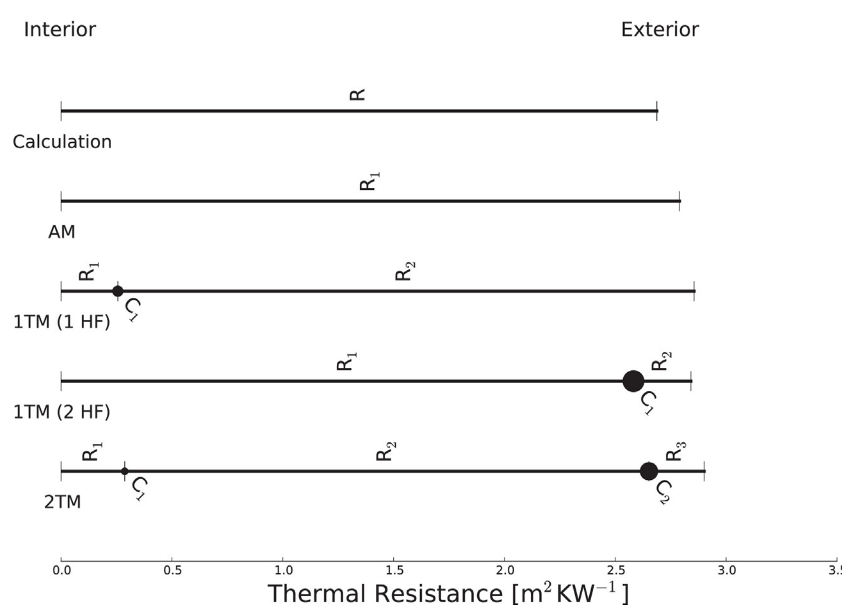

Fig. 6. Summary of the surface-to-surface R-value and size of the effective thermal mass of the TCWall as estimated with the AM and the dynamic method, with the 1TM (both using only the internal heat flux (1 HF) or both (2 HF)) and the 2TM models. The magnitude of the effective thermal mass is proportional to the radius of the solid circle. The expected R-value calculated from the manufacturer specification sheet is also shown.

resistance and U-value estimates are within error bands; the location (in thermal resistance space) of the estimated effective thermal mass varies according to heat flux measurement location. The thermal performance of this wall is distinct from that of the OWall.

Results for the 1TM (2 HF) and 2TM models identify the dominant effective thermal mass to be a relatively small thermal resistance from the external surface compared to the total thermal resistance of the wall. The 2TM model indicates a large thermal resistance separating the effective thermal masses, with a small effective thermal mass located near the interior wall surface, in thermal resistance space. This reflects the known structure of the wall (Section 2.2), which is expected to have high thermal mass layers adjacent to the surfaces. It comprises aerated clay blocks and plaster separated from a layer of gypsum fibreboard (a thin layer of high specific thermal mass material) by a total of 100 mm of woodfibre insulation (a lower thermal mass material). The characteristics of the effective thermal mass estimated by the 1TM model using only the internal heat flux measurements are dominated by the material in close proximity to the HFP [13] rather than those on the exterior side of the fibreboard insulation. The 2TM model may therefore be used to provide further insight into the structure of the wall, in effective thermal mass and resistance terms, and thus its response to heating and cooling loads on each side of the wall, as discussed in Section 5.

4.3. Model comparison

Fig. 3 suggests that the 2TM model is better at estimating the heat flow into and out of the wall compared to the 1TM model, as it indicates smaller residuals between modelled and recorded heat flux data. Both models approximate the continuous thermal resistance and mass properties of a wall through discrete components. However, through the inclusion of an additional effective thermal mass and resistance compared to the 1TM model, the 2TM model enables a better representation of different conditions and wall properties adjacent to each HFP, whilst still coupled across the whole wall depth.

Bayesian model selection (Section 3.3) was applied to the analysis for each case study to compare the performance of the 1TM (2 HF) and 2TM models and check whether the additional complexity of the 2TM model is justified. The two models were tested on the same time series used to evaluate the thermophysical properties of the elements. The natural logarithm of the odds ratio (Eq. (13)) of the 1TM to 2TM models were −14167 for the OWall and −12357 for the TCWall. In both cases the 2TM model was found to provide a substantially better representation of the recorded data than the 1TM model, suggesting that the inclusion of an additional effective thermal mass improves the physical representation of both case studies. The 2TM model enables heat flow into and out of the walls at each surface to be better represented for both the TCWall, consisting of seven different layers, and the OWall, consisting of brick and plaster.

5. Conclusions

A method to derive the thermophysical properties of a building element from in situ measurements has been developed to provide insight into its structure and performance in relation to heat flows at both interior and exterior surfaces. Heat flux and temperature measurements on both sides of building elements have been analysed using physically informed models and Bayesian statistical analysis, increasing the physical insights available from typical measurement campaigns utilising just heat flux measurement on interior surfaces [13]. Heat flows into and out of the structure of the element can be accurately characterised and the heat storage estimated, suggesting that the application of the method may be extended to different seasons and ranges of internal and external conditions (*e.g.*, heat flowing from the structure, into the structure or reversing over the monitoring period) [41].

Measurements of heat flux and temperature were taken on the internal and external surfaces of two heavy-weight walls of contrasting structure. A predominantly brick wall of standard construction (OWall), situated in an occupied office, and a well insulated clay-block-based wall (TCWall), housed in a thermal chamber, were studied. Physical models based on the electrical analogy of heat were applied to the data, assuming one-dimensional heat flow, and combined with Baysian analysis to determine the best-fit model parameters. The wall thermal properties were estimated using literature values and simple calculation; the conventional average method (AM); a one thermal mass and two thermal resistance model (1TM) with a heat flux plate on both the interior and exterior surfaces (2 HF) or one heat flux plate on the interior surface only (1 HF); and a two thermal mass, three thermal resistance model (2TM). The relative probability of the 1TM and 2TM models accurately describing the observed wall thermal performance was estimated using Bayesian model comparison.

Estimates of the in situ U-value of each wall applying different thermal mass models are within error estimates; U-value of the OWall using the AM, 1TM (1 HF), 1TM (2 HF) and 2TM models are $1.89 \pm 0.36\,\mathrm{Wm^{-2}K^{-1}}$, $1.72 \pm 0.27\,\mathrm{Wm^{-2}K^{-1}}$, $1.82 \pm 0.30\,\mathrm{Wm^{-2}K^{-1}}$ and $1.71 \pm 0.26\,\mathrm{Wm^{-2}K^{-1}}$ respectively. These values are within the broad range of possible U-values derived by simple calculation based on properties of the potential materials of the walls from literature sources, 1.11 to $2.16\,\mathrm{Wm^{-2}K^{-1}}$. Similarly, the U-values of the TCWall derived from monitored data range from $0.33 \pm 0.03\ \mathrm{Wm^{-2}K^{-1}}$ to $0.34 \pm 0.05\,\mathrm{Wm^{-2}K^{-1}}$, compared to the expected U-value estimated from the supplied properties of $0.35\,\mathrm{Wm^{-2}K^{-1}}$. The effective thermal mass estimates (Tables 1 and 2) are lower than the total thermal mass of the wall estimated from the expected structure and literature values (Section 4.1). As noted previously [13], the effective thermal mass estimates of these models do not capture the full thermal mass of the wall but rather the apparent thermal mass as seen from the perspective of the interior or exterior ambient [13]. In fact, the internal and external estimates of the effective thermal mass obtained from the 2TM model for the OWall are comparable with the calculated internal and external thermal masses reported in Section 4.1. Notably, the values calculated from tabulated data $\left(C_{\mathrm{int}} = 48,000\,\mathrm{Jm^{-2}K^{-1}}; C_{ext} = 119,000\,\mathrm{Jm^{-2}K^{-1}}\right)$ and those estimated by the dynamic method $\left(C_1 = 46,700 \pm 500\,\mathrm{Jm^{-2}K^{-1}}; C_2 = 119,100 \pm 800\,\mathrm{Jm^{-2}K^{-1}}\right)$ are in close agreement for the TCWall, where detailed information about the thermophysical properties of the building stratigraphy were available and the two effective thermal masses are clearly separated by the large thermal resistance of the woodfibre insulation.

Estimations of heat flux entering and leaving the wall were compared to the measured data for all the dynamic models. The 1TM (1 HF) model produced a good match between the modelled and measured internal heat flux, but a poor fit to the external heat flux; as expected the dynamic behaviour is optimised at the measurement location of heat flux. The 1TM (2 HF) model produced a better match to the exterior heat flux measurements than the 1 HF model, but a worse fit to the interior heat flux. This is not surprising, as the available data exceeds the parameterisation of the model exposing the inability of the simple 1TM model to accurately represent the thermal performance of heavy-weight walls at both surfaces. However, the 2TM model provided a good fit to both the internal and external heat flux for both walls. In line with these results, the odds ratio calculated for Bayesian model selection indicate that the 2TM model has a much higher probability of representing the observed data than the 1TM (2 HF) model for both walls (noting that the same data is required for application of model comparison).

The 1TM (1 HF) model estimated effective thermal mass close to the interior surface for the OWall and TCWall and it may be used to provide insight into the dynamic performance of the interior space and inform a retrofitting and space heating strategy. The 1TM (2 HF) model estimated the effective thermal mass to be nearer to external surface for both the OWall and TCWall; as noted above, the underparameterisation of the model has led to a poorer fit of heat flux data at the internal surface and this effective thermal mass would be of limited use to estimate the thermal performance of the interior space. The 2TM model places the effective thermal masses close to the surfaces for both the OWall and TCWall; however, the relative sizes of the thermal resistances are different for these walls and reflects the known physical structure of the walls. Knowledge of the estimated size and locations of the effective thermal mass and thermal resistances may be valuable for design purposes. For example, to tailor retrofitting solutions, where the structure of a building element is often not well characterised [13,32], and to determine the performance of the interior space both during the heating season and during periods of high external temperatures, potentially informing the cooling strategy of buildings.

The development of an enhanced model to estimate the thermophysical properties of building elements using a physically representative model based on the electrical analogy to heat and Bayesian statistics, and using in situ measured data, supports greater understanding of the performance of building elements. The ability to account for both heat flow into and out of a building element supports an extension of the seasons in which such measurement campaigns may be undertaken, and the potential to account for direct solar radiation [41]. The two thermal mass, three thermal resistance model may be applied to support improved thermal comfort and energy performance through helping close the performance gap, informing tailored retrofitting solutions and both space heating and cooling strategies.

Acknowledgements

This research was made possible by support from the EPSRC Centre for Doctoral Training in Energy Demand (LoLo), grant numbers EP/L01517X/1 and EP/H009612/1, and the RCUK Centre for Energy Epidemiology (CEE), grant number EP/K011839/1. The study in the environmental chamber was supported by funding from Natural Building Technologies and Technology Strategy Board. All data used in this research are openly available at [50,51]. The authors are grateful to Prof. Robert Lowe for helpful discussions and to Cameron Scott and Caroline Rye of Archimetrics Ltd for their help during the installation of equipment on the office wall.

References

[1] S. de Wit, Uncertainty in building simulation, in: Advanced Building Simulation, Taylor & Francis, Abingdon, UK, 2004.
[2] A. Stone, D. Shipworth, P. Biddulph, T. Oreszczyn, Key factors determining the energy rating of existing English houses, Build. Res. Inf. 42 (6) (2014) 725–738, http://dx.doi.org/10.1080/09613218.2014.905383, ISSN: 0961-3218.
[3] M. Hughes, J. Palmer, V. Cheng, D. Shipworth, Global sensitivity analysis of England's housing energy model, J. Build. Perform. Simul. 8 (5) (2015) 283–294, http://dx.doi.org/10.1080/19401493.2014.925505, ISSN: 1940-1493.
[4] J.R. Stein, A. Meier, Accuracy of home energy rating systems, Energy 25 (4) (2000) 339–354, http://dx.doi.org/10.1016/S0360-5442(99)00072-9, ISSN: 0360-5442.
[5] Zero Carbon Hub, Closing the gap between design & as-built performance, End of term report, Tech. Rep., 2014.
[6] M. Delghust, W. Roelens, T. Tanghe, Y.D. Weerdt, A. Janssens, Regulatory energy calculations versus real energy use in high-performance houses, Build. Res. Inf. 43 (6) (2015) 675–690, http://dx.doi.org/10.1080/09613218.2015.1033874.
[7] C. van Dronkelaar, M. Dowson, C. Spataru, D. Mumovic, A review of the regulatory energy performance gap and its underlying causes in non-domestic buildings, Indoor Environ. 1 (2016) 17, http://dx.doi.org/10.3389/fmech.2015.00017.
[8] P.G. Cesaratto, M. De Carli, A measuring campaign of thermal conductance in situ and possible impacts on net energy demand in buildings, Energy Build. 59 (2013) 29–36, http://dx.doi.org/10.1016/j.enbuild.2012.08.036, ISSN: 0378-7788.
[9] F.G.N. Li, A. Smith, P. Biddulph, I.G. Hamilton, R. Lowe, A. Mavrogianni, E. Oikonomou, R. Raslan, S. Stamp, A. Stone, A. Summerfield, D. Veitch, V. Gori, T. Oreszczyn, Solid-wall U-values: heat flux measurements compared with standard assumptions, Build. Res. Inf. 43 (2) (2014) 238–252, http://dx.doi.org/10.1080/09613218.2014.967977, ISSN: 0961-3218.
[10] P. de Wilde, The gap between predicted and measured energy performance of buildings: a framework for investigation, Autom. Constr. 41 (2014) 40–49, http://dx.doi.org/10.1016/j.autcon.2014.02.009, ISSN: 0926-5805.
[11] F. Xeni, P. Eleftheriou, I. Michaelides, S. Hadjiyiannis, P. Philimis, A. Stylianou, In situ U-value measurements for today's Cypriot houses, Int. J. Sustain. Energy 34 (3–4) (2015) 248–258, http://dx.doi.org/10.1080/14786451.2014.882334, ISSN: 1478-6451.
[12] B. Anderson, Site-testing thermal performance: a CIB survey, Batiment Int. Build. Res. Pract. 12 (3) (1984) 147–149.
[13] P. Biddulph, V. Gori, C.A. Elwell, C. Scott, C. Rye, R. Lowe, T. Oreszczyn, Inferring the thermal resistance and effective thermal mass of a wall using frequent temperature and heat flux measurements, Energy Build. 78 (2014) 10–16, http://dx.doi.org/10.1016/j.enbuild.2014.04.004, ISSN: 0378-7788.
[14] G. Litti, S. Khoshdel, A. Audenaert, J. Braet, Hygrothermal performance evaluation of traditional brick masonry in historic buildings, Energy Build. 105 (2015) 393–411, http://dx.doi.org/10.1016/j.enbuild.2015.07.049, ISSN: 0378-7788.
[15] C. Bankvall, Forced convection: practical thermal conductivity in an insulated structure under the influence of workmanship and wind, in: Thermal Transmission Measurements of Insulation, 660, ASTM International, 1978, pp. 409–425.
[16] S. Rouchier, M. Woloszyn, Y. Kedowide, T. Béjat, Identification of the hygrothermal properties of a building envelope material by the covariance matrix adaptation evolution strategy, J. Build. Perform. Simul. 9 (1) (2016) 101–114, http://dx.doi.org/10.1080/19401493.2014.996608, ISSN: 1940-1493.
[17] P. Wouters, L. Vandaele, P. Voit, N. Fisch, The use of outdoor test cells for thermal and solar building research within the PASSYS project, Build. Environ. 28 (2) (1993) 107–113, http://dx.doi.org/10.1016/0360-1323(93)90044-4, ISSN: 0360-1323.
[18] P.H. Baker, H.A.L. van Dijk, PASLINK and dynamic outdoor testing of building components, Build. Environ. 43 (2) (2008) 143–151, http://dx.doi.org/10.1016/j.buildenv.2006.10.009, ISSN: 0360-1323.
[19] IEA, IEA EBC Annex 58, Reliable Building Energy Performance Characterisation Based on Full Scale Dynamic Measurements, 2011.
[20] G. Stevens, J. Bradford, Do U-Value Insulation? England's Field Trial of Solid Wall Insulation, in: ECEEE Summer Study Proceedings, 2013, pp. 1269–1280.
[21] Energy Saving Trust, CE128/GIR64: Post-Construction Testing – A Professionals Guide to Testing Housing for Energy Efficiency, 2005.
[22] A. Rabl, Parameter estimation in buildings: methods for dynamic analysis of measured energy, J. Solar Energy Eng. 110 (1988) 52–66.
[23] U. Norlén, Estimating thermal parameters of outdoor test cells, Build. Environ. 25 (1) (1990) 17–24, http://dx.doi.org/10.1016/0360-1323(90)90036-Q, ISSN: 0360-1323.
[24] M.J. Jiménez, B. Porcar, M.R. Heras, Application of different dynamic analysis approaches to the estimation of the building component U value, Build. Environ. 44 (2) (2009) 361–367, http://dx.doi.org/10.1016/j.buildenv.2008.03.010, ISSN: 0360-1323.
[25] I. Naveros, P. Bacher, D.P. Ruiz, M.J. Jiménez, H. Madsen, Setting up and validating a complex model for a simple homogeneous wall, Energy Build. 70 (2014) 303–317, http://dx.doi.org/10.1016/j.enbuild.2013.11.076, ISSN: 0378-7788.
[26] D. Coakley, P. Raftery, M. Keane, A review of methods to match building energy simulation models to measured data, Renew. Sustain. Energy Rev. 37 (2014) 123–141, http://dx.doi.org/10.1016/j.rser.2014.05.007, ISSN: 1364-0321.
[27] R. Kramer, J. van Schijndel, H. Schellen, Simplified thermal and hygric building models: a literature review, Front. Arch. Res. 1 (4) (2012) 318–325, http://dx.doi.org/10.1016/j.foar.2012.09.001.
[28] N.R. Kristensen, H. Madsen, S.B. Jørgensen, Parameter estimation in stochastic grey-box models, Automatica 40 (2) (2004) 225–237, http://dx.doi.org/10.1016/j.automatica.2003.10.001, ISSN: 0005-1098.
[29] BS ISO 9869-1, Thermal Insulation – Building Elements – In-Situ Measurement of Thermal Resistance and Thermal Transmittance. Part 1: Heat Flow Meter Method, 2014.
[30] D.J. MacKay, Information Theory, Inference, and Learning Algorithms, 4th ed., Cambridge University Press, Cambridge (UK), 2003.
[31] Hukseux, HFP01 Heat Flux Plate, 2015 http://www.hukseflux.com/product/hfp01.
[32] C. Rye, The SPAB – U-value report, Tech. Rep. 1, 2012.

[33] Campbell Scientific, CR1000 Measurement and Control Datalogger, 2015, https://www.campbellsci.co.uk/cr1000.
[34] V. Marincioni, H. Altamirano-Medina, I. Ridley, Performance of internal wall insulation systems – experimental test for the validation of a hygrothermal simulation tool, in: Proceedings of Nordic Symposium on Building Physics, Lund, Sweden, 2014.
[35] Campbell Scientific, CR3000 Micrologger, 2015 https://www.campbellsci.co.uk/cr3000.
[36] Eltek, Squirrel 450/850 Series Data Logger, 2015 http://www.eltekdataloggers.co.uk/450_series.html.
[37] G.J. Levermore, J.B. Parkinson, Analyses and algorithms for new Test Reference Years and Design Summer Years for the UK, Build. Serv. Eng. Res. Technol. 27 (4) (2006) 311–325, http://dx.doi.org/10.1177/0143624406071037, ISSN: 0143-6244, 1477-0849.
[38] T. Oreszczyn, S.H. Hong, I. Ridley, P. Wilkinson, The Warm Front Study Group, Determinants of winter indoor temperatures in low income households in England, Energy Build. 38 (3) (2006) 245–252, http://dx.doi.org/10.1016/j.enbuild.2005.06.006.
[39] B.P. Lathi, R.A. Green, Essentials of Digital Signal Processing, Cambridge University Press, 2014, ISBN 978-1-107-05932-0.
[40] W.M. Siebert, Circuits, Signals and Systems, MIT Press, 1986, ISBN: 978-0-262-19229-3.
[41] V. Gori, A novel method for the estimation of thermophysical properties of walls from short and seasonal-independent in-situ surveys (PhD), University College London, London, UK, 2017 (in press).
[42] P. Gregory, Bayesian Logical Data Analysis for the Physical Sciences – A Comparative Approach with Mathematica Support, Cambridge University Press, New York, USA, 2005.
[43] D.J. Wales, J.P. Doye, Global optimization by basin-hopping and the lowest energy structures of Lennard-Jones clusters containing up to 110 atoms, J. Phys. Chem. A 101 (28) (1997) 5111–5116, http://dx.doi.org/10.1021/jp970984n.
[44] H. Jeffreys, S. Santosh, The Theory of Probability, OUP Oxford, 1998 Reissue ed., 1939, ISBN 1-139-84822-4.
[45] I.J. Good, Corroboration, explanation, evolving probability, simplicity and a sharpened razor, Br. J. Philos. Sci. 19 (2) (1968) 123–143, ISSN: 0007-0882.
[46] W.H. Jefferys, J.O. Berger, Ockham's Razor and Bayesian analysis, Am. Sci. 80 (1) (1992) 64–72, ISSN: 0003-0996.
[47] CIBSE, Environmental Design – Guide A, 2007.
[48] BS EN ISO 6946, Building Components and Building Elements – Thermal Resistance and Thermal Transmittance – Calculation Method, 2007.
[49] EN ISO 13786, Thermal Performance of Building Components – Dynamic Thermal Characteristics – Calculation Methods, 2008.
[50] V. Gori, C. Elwell, In-situ measurements of heat flux and temperature on a solid-brick wall in office building, 2016 [Dataset]. Available at: http://discovery.ucl.ac.uk/1526521/.
[51] V. Marincioni, H. Altamirano, Measurement of heat flux and temperature on a solid wall in an environmental chamber, 2016 [Dataset]. Available at: http://discovery.ucl.ac.uk/1527422/.